Plant Sci. Arc.
Plant Science Archives
An International Journal of Plant Biology

Original Research Article
ISSN 2518-6965
Journal Homepage: www.plantarc.com

Investigation of toxicity from *Hibiscus lobatus* (Murray) Kuntze leaf extract through plant-based Zinc oxide metallic nanoparticles and their applications

Darshan R C and Siddappa B Kakkalameli*

Department of Studies in Botany, Davangere University, Karnataka – 577007, India

Citation: Darshan R C and Siddappa B Kakkalameli (2025). Investigation of toxicity from *Hibiscus lobatus* (Murray) Kuntze leaf extract through plant-based Zinc oxide metallic nanoparticles and their applications. *Plant Science Archives.*
DOI: https://doi.org/10.51470/PSA.2025.10.3.91

Corresponding Author: **Siddappa B Kakkalameli** | E-Mail: **(siddubotdu@davangereuniversity.ac.in)**

Received 21 June 2025 | Revised 23 July 2025 | Accepted 18 August 2025 | Available Online 23 September 2025

ABSTRACT

Nanoparticles derived from plants hold immense promise across disciplines such as agriculture and medicine due to their antimicrobial and anticancer capabilities. So, from rising concerns due to their potential adverse effects—commonly referred to as nanotoxicity—which may lead to phytotoxic responses in crops and pose ecological risks through accumulation in biological systems. This method utilizes Zn $(NO_3)_2.6H_2O$ and bioactive compounds from the Aqueous leaf extract, ensuring a non-toxic process. The Integrated samples were thoroughly characterized using various techniques, including UV-visible spectroscopy, FTIR, XRD, EDX, Zeta potential analysis, SEM, TEM, and DLS, all of which confirmed their structure and stability. The formation of nanoparticles was confirmed by UV-visible spectroscopy, which displayed a characteristic surface plasmon resonance (SPR) band at 374 nm. Furthermore, FTIR analysis revealed the presence of key functional groups, including those corresponding to alcohols, carboxylic acids, and amine salts. isothiocyanates, aromatic compounds, conjugated alkenes, aldehydes, and halo compounds, highlighting the role of bioactive components in nanoparticle synthesis. XRD analysis confirmed a spherical crystalline structure, while EDX analysis determined the elemental composition of Zinc (41.8%), Nitrogen (14.7%), and Oxygen (38.4%). SEM analysis measured the nanoparticle size at 40 nm, with a potential Zeta value of +6.6 mV and DLS measurement of 145.2 nm, ensuring stability and uniformity. The exhibited antioxidant, antimicrobial, antifungal, anti-diabetic, and anti-cancer properties, demonstrating their potential for biomedical applications. Their effectiveness against Staphylococcus aureus, Pseudomonas aeruginosa, Aspergillus flavus, and Pichia anomala is notable, with anti-bacterial and anti-fungal properties. The potential therapeutic relevance of these materials is highlighted by their anti-cancer activity observed against the MCF-7 and A549 cell lines. This investigation details a sustainable and cost-effective approach for the eco-friendly synthesis of Zinc Oxide Nanoparticles (ZnO NPs) using an aqueous leaf extract of Hibiscus lobatus. Ultimately, these results indicate that the plant-mediated compounds could function as viable, promising alternatives within nanomedicine, thereby fostering progress in healthcare and biomedical research.

Keywords: *Anti-cancer activity, green synthesis, Hibiscus lobatus, Phytochemical, Zinc oxide nanoparticles.*

1. INTRODUCTION

The Malvaceae, Family commonly known for mallow family, consists of erect, woody plants with large, variably colored flowers [1]. Reported to include about 80 genera and over 1,000 species worldwide, most members are widespread, especially in South America, except in icy regions [2] Malvaceae, with around 85 genera and between 1,000 and 1,500 species, is broadly distributed across tropical and temperate zones, including 22 genera and approximately 125 species from India [3]. This family comprises nearly 243 genera with 4,225 species of flowering plants [4]. In India, about 35 Hibiscus species fall into 10 sections [5]. Nanotechnology has focused on minuscule particles ranging from 1 to 100 nanometers that possess unique properties. Due to their large surface area and small sizes, they are vital across healthcare, technology, and environmental sciences, used for drug delivery systems, catalysis, and sensors [6]. Nanoparticles show promise in combating antimicrobial resistance through the production of superoxide, hydroxyl ions, and free radicals, and can kill bacteria by damaging cellular components, thereby offering potential solutions for controlling resistant infections and wound management [7]. They play an important role in technological progress, improving the quality of life and environmental sustainability.

Plant-mediated nanoparticle synthesis via green chemistry provides an eco-friendly alternative by developing processes and materials that avoid harmful substances. This approach prevents pollution at its source rather than dealing with it after it occurs, focusing on waste reduction and energy efficiency. This is a cost-effective method that integrates nanotechnology with phyto-biotechnology. Bioactive phytochemicals in botanical extracts—such as flavonoids, alkaloids, tannins, terpenoids, and phenolics—act as reducing, capping, and stabilizing agents, enabling controlled synthesis with enhanced properties. This method eliminates hazardous chemicals, reduces toxicity, and lessens environmental impact, making it a preferable alternative to traditional methods [8]. Nanoparticles enhance the bioavailability and therapeutic efficacy of natural and synthetic antioxidants, especially those with poor solubility, by covalently binding them, encapsulating them, or incorporating them into nanostructures, which protects against degradation and boosts their ability to combat oxidative stress [9]. The well-established role of Zinc oxide nanoparticles (ZnO-NPs) in managing oxidative stress and inhibiting microbial activity stems from their capacity to neutralize detrimental species, notably superoxide radicals, hydroxyl radicals, and hydrogen peroxide.to protect cells and tissues from oxidative damage.

They also disrupt microbial cell mechanisms like DNA replication, protein synthesis, and cell division, making them important in therapeutic and biomedical applications [10]. In the context of diabetes management, the enhanced surface area and nanoscale properties of these agents allow them to effectively regulate blood glucose and enhance insulin sensitivity. They contribute to glycemic control by inhibiting key carbohydrate-metabolizing enzymes, specifically α-amylase and α-glucosidase, which consequently reduces glucose absorption [11]. An inherent antioxidant properties offer protection to pancreatic β-cells against oxidative stress, a critical mechanism in the advancement of diabetes [12]. ZnO NPs synthesized with extracts from *Boerhaavia diffusa* and *Tamarindus indica* exhibit significant α-amylase inhibition, supporting their role in glucose regulation. Additionally, leaf extracts of medicinal plants such as *Azadirachta indica*, *Hibiscus rosa-sinensis, Murraya koenigii, Moringa oleifera*, and *Tamarindus indica* show remarkable antidiabetic and antioxidant activities, with reduced toxicity and adverse effects [13]. Incorporating ZnO NPsinto nanofibers enhances diabetes treatment by improving bioavailability and efficacy, enabling better glucose regulation, and addressing complications like infections and inflammation. Furthermore, ZnO NPsshow promise in cancer therapy by targeting malignant cells selectively, mainly through generating reactive oxygen species that induce oxidative stress and apoptosis, as well as disrupting cellular regulation via elevated zinc ions. They serve as efficient drug carriers, improving targeted delivery to tumors. Despite their potential, clinical use is still limited due to insufficient in vivo studies and concerns about bioavailability and toxicity. Advancing their application requires Unity across disciplines such as oncology, biology, and materials science to optimize designs and efficacy. With ongoing research, ZnO NPscould be a significant therapy that spares healthy tissues, especially when integrated into drug delivery systems [14]. Cancer, characterized by uncontrolled cell growth, involves the proliferation of abnormal cells capable of invading nearby tissues and spreading to distant organs via metastasis, leading to high mortality rates (WHO). The MCF-7 (Breast cancer) cell line, derived in 1970 from a pleural effusion of a 69-year-old woman, Frances Mallon, with metastatic breast adenocarcinoma, expresses estrogen, progesterone, and glucocorticoid receptors, making it a valuable model for hormone-responsive breast cancer studies [15]. The A549 (Lung cancer) cell line, which originated from the human alveolar basal epithelium of a 58-year-old Caucasian male's lung cancer tissue and was established by Giard in 1972, is commonly employed to model water and electrolyte diffusion across the alveolar membrane [16]. This line, along with the MCF-7 line, is one of two key models extensively used in cancer research to investigate tumor progression, drug responses, and potential treatment strategies. In the current work, Zinc Oxide Nanoparticles (ZnO NPs) were green-synthesized using *H. lobatus* leaf extracts, resulting in the designated *H. lobatus* ZnO NPs. A comprehensive panel of analytical methods—including UV–Visible spectroscopy, FTIR, XRD, DLS, SEM, zeta potential, TEM, and EDX—was used to fully characterize their physicochemical properties, such as shape, size, morphology, stability, and crystal structure. Following characterization, the antioxidant activity was quantified using the DPPH assay, the anti-microbial activity was assessed by the well diffusion method, and the anti-diabetic potential was determined via α-glucosidase inhibition.

Finally, their anti-cancer effects were investigated against the MCF-7 and A549 cell lines using the MTT assay.

2. Materials and methodology of *Hibiscus lobatus* ZnO NPs

2.1 Collection and processing of *Hibiscus lobatus* Plant Material:

The Fresh *Hibiscus lobatus* leaves were meticulously gathered from the Jambooti Forest in the Kanpaur district of Karnataka, India (Figure 01). following proper identification and validation. From GKVK Bengaluru, and assigned an accession number USAB 5610. Initially, the leaves are washed with flowing water. The leaves were initially rinsed with tap water to eliminate debris and organic contaminants, followed by a final rinse with distilled water. To maximize the retrieval of bioactive compounds, approximately 25 grams of the leaf powder was subjected to Soxhlet extraction using 250 mL of distilled water. After extraction, the resulting crude solution was allowed to cool to ambient temperature. It was then filtered through Whatman filter paper to remove residual particulates. The final filtered extract was stored under refrigeration at 4 ^{0}C for subsequent systematic application.

Qualitative Phytochemical Analysis

List 1: Method of Qualitative Estimation

Analysis/Activity	Methods
Phytochemical Analysis Phenols, Phenols, Alkaloids, Flavonoids, Tannins, Terpenoids, Saponins, Glycosides, Steroids, Proteins, Carbohydrates.	[17]

AOAC: Association of Official Analytical Chemists.

2.3 GC–MS analysis of *Hibiscus lobatus* Aq. Extract

The aqueous leaf extracts of *Hibiscus lobatus* were subjected to GC-MS to determine their phytochemical constituents by standard procedures, using a Shimadzu QP2010S system operating The analysis was performed using Gas Chromatography-Mass Spectrometry (GC-MS) with an electrospray ionization (ESI) mode interface. The system was fitted with an ELITE-5MS capillary column (30 m length, 0.25 mm internal diameter, 0.25 µm film thickness). The GC oven temperature was initially set at 80 ∘C, then increased at a rate of 20 ∘C per minute up to 450 ∘C to achieve optimal analyte separation. Samples were introduced via a 2 mm direct injection technique. Compound identification relied on comparing the relative retention times and mass spectral data with authenticated reference spectra housed within the National Institute of Standards and Technology (NIST) library. This analytical approach followed established methodology to ensure accurate compound characterization, consistent with the protocol outlined by [18].

2.4 Formulation of ZnO NPs from the aqueous leaf extracts of H*. lobatus*

Zinc oxide nanoparticles (ZnO NPs) were prepared using an eco-friendly method involving a green synthesis approach. This procedure blended an aqueous 0.01 M zinc nitrate hexahydrate ($Zn(NO_3)2{\cdot}6H_2O$) solution (98% purity, procured from NICE Chemicals, Karnataka, India) with *H. lobatus* leaf extract. For the synthesis, 5 mL of the *H. lobatus* extract was combined with 95 mL of the 0.01 M zinc nitrate solution. This mixture was magnetically stirred at 75 ∘C and 150 rpm for one hour to facilitate the bio-reduction process and subsequent formation of the ZnO NPs. The resultant nanomaterial was then isolated by centrifugation at 5000 rpm for 25 minutes.

After decanting the supernatant, the precipitated ZnO NPs were thoroughly washed with distilled water and reserved for future characterization and applications [19]. The complete synthesis and characterization pathway for the ZnO NPs is illustrated in (Figure 02).

2.5 Characterization of *H. lobatus Zinc* Oxide Nanoparticles (ZnO NPs):

The characterization of the biosynthesized *Hibiscus lobatus*–mediated ZnO nanoparticles was carried out by standard protocols, ensuring comprehensive evaluation of their physicochemical and structural attributes by (20). (21) (22) (23)(24). (25). UV-Vi's spectra were measured using a double-beam UV-9600 A spectrophotometer (Shanghai, China) in the range of 200 to 600nm. The FTIR study spectrophotometer (Thermo Fisher Scientific, Waltham, MA, USA) mixed the ZnO NPs with potassium bromide (KBr). The synthesized material underwent comprehensive characterization, beginning with Fourier-Transform Infrared (FTIR) spectroscopy, where the sample was embedded in a KBr pellet and analyzed across the 400 to 4000 cm−1 wavenumber range. For X-ray diffraction (XRD), patterns were collected using a Rigaku Miniflex 600 diffractometer at 40 kV and 30 mA with Cu Kα radiation across a 2θ range of 20◦ to 80◦. Scanning Electron Microscopy (SEM), coupled with an Energy-Dispersive X-ray (EDX) system (JEOL JSM IT 500 LA), involved placing the plant extract onto a carbon-taped stub, which was subsequently gold-plated via sputter deposition for imaging. Zeta potential measurements were performed on an ultrasonicated and centrifuged (6000 rpm for 20 min) suspension of the ZnO NPs using a Horiba Scientific Nanoparticle Analyzer at 3.4 eV. The hydrodynamic size and dispersion of the *H. lobatus* ZnO nanoparticles were concurrently determined using Dynamic Light Scattering (DLS). Finally, Transmission Electron Microscopy (TEM) analysis was conducted using a FEI TECNAI G2 F30 to assess the size, morphology, and structure; this involved drying 5 µL of the NPs on a TEM grid for 48 hours and scanning at 300 keV, with images acquired at resolutions between 7000× and 8000.

2.6 Anti-microbial activity of *H. lobatus* ZnO NPsby a well diffusion method:

The antimicrobial activity of the *H. lobatus*–derived ZnO nanoparticles (HL-ZnO NPs) was evaluated using the standard well diffusion assay(26). The nanoparticles were tested against a panel of pathogenic organisms: the Gram-positive bacterium *Staphylococcus aureus* (MTCC-7443), the Gram-negative bacterium *Pseudomonas aeruginosa* (MTCC-1034), and the fungal species *Aspergillus flavus* (MTCC-9606) and *Pichia anomala* (MTCC-237). The microbial inoculum for each strain was adjusted to a density of approximately 5×10^5 CFU/mL using a sterile saline solution. A 20 mg/mL stock solution of the HL-ZnO NPs was prepared in DMSO. Varying concentrations, ranging from 100 to 400 µg, were loaded into separate wells cut into the agar medium. Muller-Hinton agar was used as the growth medium for bacterial cultures, while Czapek-Dox agar was employed for the fungal species. Bacterial plates were incubated at 37 °C for 24 hours, and fungal plates were incubated at 28 °C for 72 hours. Following incubation, the HL-ZnO NP's efficacy was quantified by measuring the diameter of the zone of inhibition in millimeters.

2.7 DPPH assay of *H. lobatusZnO NPs*

The radical-scavenging potential of *H. lobatus* zinc oxide (ZnO) nanoparticles was examined using the stable DPPH radical assay, adapted from (27). ZnO NPs concentrations were prepared within a range of 0 to 250 µg/mL, and 2 mL of 100 µM DPPH solution was mixed with *H. lobatus* ZnO NPs, with the final volume adjusted to 3 mL using methanol. The reaction mixtures were incubated in a dark environment at ambient temperature for 45 minutes. Absorbance was recorded at 517 nm employing a Shimadzu UV-1800 spectrophotometer, with a blank solution (excluding sample/standard) serving as the reference control. The free radical neutralization activity was calculated and represented as IC_{50} values, with vitamin C utilized as the benchmark antioxidant.

2.8 Inhibitory activity against α-Glucosidase from *H. lobatus ZnO* NPs

The α-glucosidase inhibitory activity of the *Hibiscus lobatus* ZnO NPs was evaluated using a standard photometric method [28]. The procedure involved dissolving 50 µL of α-glucosidase (1 U/mL from yeast) in 50 mM phosphate buffer (pH 6.9). This enzyme solution was then incubated with varying concentrations of the *H. lobatus* ZnO nanoparticles (ranging from 0 to 125 µg/mL) for 10 minutes at 37 °C. The enzymatic reaction was initiated by the addition of 50 µL of 5 mM p-nitrophenyl-D-glucopyranoside in the same phosphate buffer. After an incubation period of 30 minutes at 37 °C, the reaction was halted by introducing 1 M sodium carbonate (Na_2CO_3). The resulting absorbance was subsequently measured at 405 nm. The inhibition percentage was calculated to determine the IC_{50} values, with Acarbose serving as the positive control.

2.9 Cytotoxicity property of *H. lobatus* ZnO NPsby MTT assay

The MTT assay is a widely utilized colorimetric technique for assessing cell viability, proliferation, and cytotoxicity. This method relies on the enzymatic reduction of the yellow, water-soluble tetrazolium dye (MTT) into insoluble formazan crystals by metabolically active cells. The reduction process is facilitated by mitochondrial dehydrogenase enzymes, which are essential for cellular respiration and energy metabolism. Upon completion of the reaction, the formazan crystals are solubilized using an appropriate organic solvent. This reaction yielded a purple-colored solution, where the intensity of the coloration corresponded proportionally to the number of metabolically active, viable cells. Allowing for quantitative measurement using a spectrophotometer at 570 nm [29-30].

3. RESULTS AND DISCUSSION

3.1 Preliminary qualitative phytochemical analysis of *Hibiscus lobatus* Leaf extracts

Table 01: Qualitative phytochemical estimation of H. lobatus leaf extract samples

Sl No	Phytochemical tests	HLLFM	HLLFDW	HLLFPE
1	Phenols	+	+	+
2	Alkaloids	+	+	+
3	Flavonoids	+	+	+
4	Tannins	+	+	+
5	Terpenoids	+	+	+
6	Saponins	+	+	-
7	Glycosides	-	+	-
8	Steroids	+	-	-
9	Proteins	+	+	+
10	Carbohydrates	+	+	+

NOTE: + Present and - Absent. M=Methanol, DW=Distilled water, PE=Petroleum ether HLLF-Hibiscus lobatus Leaf

The phytochemical analysis of *Hibiscus lobatus* leaf extracts aligns with FTIR findings, confirming the presence of phenols, alkaloids, flavonoids, tannins, terpenoids, saponins, glycosides, proteins, and carbohydrates. These bioactive compounds play a prominent role in reducing zinc nitrate and controlling nanoparticle size during synthesis. The methanolic extract of *H. lobatus* leaves contains alkaloids, flavonoids, tannins, phenols, carbohydrates, and proteins, indicating its rich phytochemical profile. In contrast, the distilled water extract lacks steroids, while the petroleum ether extract retains most compounds except for saponins, glycosides, and steroids. Notably, saponins and glycosides also exhibit the absence of steroids, as outlined in Table 1.

3.2 GC-MS Analysis of *H. lobatus* Aqueous Leaf Extract:

The intracellular metabolites of *H. lobatus* were analyzed using gas chromatography-mass spectrometry (GC–MS). The chromatogram revealed 15 compounds. (Figure 03). shows a chromatogram with peaks. The associated compounds are presented in Table 02. The GC–MS chromatogram revealed that the major compounds identified were 2-Hexadecen-1-ol, 3,7,11,15-tetramethyl-, acetate (34,14%), Hexadecanoic acid, methyl ester (10.27%), which was identified as a key compound, known for its antioxidant and antimicrobial properties. Similarly, Hexadecanoic acid, methyl ester (10.27%) has been reported to possess anti-inflammatory and lipid-lowering effects, making it valuable in cardiovascular health applications. 9,12-Octadecadienoic acid (Z, Z)-, methyl ester (5.91%), a polyunsaturated fatty acid, suggests its role in reducing oxidative stress and improving metabolic functions. Lanosterol (3.99%), a precursor in steroid biosynthesis with potential anti-inflammatory effects (31). Gamma-sitosterol (10.23%), additionally, gamma-sitosterol (10.23%) is widely recognized for its cholesterol-lowering and anticancer potential, as demonstrated in previous studies on plant-derived sterols. Squalene (5.10%), a well-known precursor in sterol biosynthesis, has been linked to skin protection and immune modulation. Stigmasterol (2.89%) further supports the pharmacological relevance of *H. lobatus*, as these compounds have been associated with antidiabetic and anticancer activities. (32) 2-Pentadecanone, 6,10,14-trimethyl- (5.07%). Lanosta-8,24-dien-3-one (2.97%), these compounds are shown (Figure 04). They were found to exhibit significant bioactivities, including antioxidant, antimicrobial, antidiabetic, and anticancer properties. The findings from the GC-MS analysis confirm that *H. lobatus* contains a diverse range of bioactive metabolites, reinforcing its potential for therapeutic applications. These results align with previous literature on medicinal plants, highlighting their role in natural drug discovery and disease prevention. An investigational studies are necessary to validate the pharmacological efficacy of these compounds.

Table 02: showing a Peak report of H. lobatus Leaf extract through GC-MS analysis

Peak#	R. Time	Area	Area%	Similarity	Base m/z	CAS#	Name
1	13.892	916706	1.22	95	111.05	17092-92-1	2(4H)-Benzofuranone, 5,6,7,7a-tetrahydro-4,4,7a-trimethyl-,
2	16.641	1034475	1.37	93	43.00	5989-02-6	Loliolide
3	16.875	1432021	1.90	90	74.05	62691-05-8	Tetradecanoic acid, 12-methyl-, methyl ester, (S)-
4	17.518	3827263	5.07	94	43.05	502-69-2	2-Pentadecanone, 6,10,14-trimethyl-
5	18.708	1646326	2.18	88	43.05	10030-74-7	Methyl hexadec-9-enoate
6	18.801	7749181	10.27	95	74.05	112-39-0	Hexadecanoic acid, methyl ester
7	19.360	1021918	1.35	93	73.00	57-10-3	n-Hexadecanoic acid
8	21.591	4459055	5.91	94	67.05	112-63-0	9,12-Octadecadienoic acid (Z, Z)-, methyl ester
9	21.691	8733134	11.58	95	79.05	301-00-8	9,12,15-Octadecatrienoic acid, methyl ester, (Z, Z, Z)-
10	21.886	25757543	34.14	93	71.05	10236-16-5	2-Hexadecen-1-ol, 3,7,11,15-tetramethyl-, acetate, (R- (R*, R*
11	32.885	3847803	5.10	96	69.05	111-02-4	Squalene
12	38.585	2182535	2.89	88	83.05	83-48-7	Stigmasterol
13	39.442	7718571	10.23	90	43.05	83-47-6	gamma. -Sitosterol
14	39.594	2104570	2.79	81	69.05	5539-04-8	Lanosta-8,24-dien-3-one
15	40.164	3012605	3.99	86	69.05	79-63-0	Lanosterol

Note: R.time=Retenation time, CAS=Chemical abstract services,

3.3 Characterization of *H. lobatus* :ZnO NPsresults:

3.3.1 UV-Vi's analysis of *H. lobatus* ZnO Nanoparticles

ZnONPs were formulated from an aqueous extract of *H. lobatus* leaves. The color change from brownish-red to pale yellow after adding zinc nitrate solution and incubating for 24 hours, the successful synthesis was confirmed at ambient temperature (27 °C) under pH 8.0 conditions. UV–Visible absorbance was recorded across the spectral range of 200–800 nm [33]. The characteristic surface plasmon resonance (SPR) absorption spectrum was observed at 374 nm (Figure 05). The high absorbance at 374 nm suggests that the synthesizedZnO NPs possess excellent optical properties, which are suitable for applications in photocatalysis, biosensing, and optoelectronic devices. The findings coordinate with previous research on green-synthesized ZnO nanoparticles, emphasizing their biocompatibility and environmental sustainability [34]. Similar results were obtained from the plant *Deverratortuosa using* ZnO NPs, where a comparable SPR absorption peak was observed, reinforcing the consistency of plant-mediated ZnO nanoparticle synthesis [35] confirming the green synthesis of *H. lobatus* ZnO nanoparticles. It is described that the UV-visible spectrum absorption peak intensity correlates with nanoparticle size. The optical properties of ZnO nanoparticles are largely influenced by their particle size, shape, and surface functionalization, which determine their bandgap energy and photonic behavior. Studies indicate that smaller ZnO nanoparticles exhibit blue-shifted absorption peaks, whereas larger nanoparticles tend to show red-shifted peaks, due to quantum confinement effects [36].

3.3.2 FTIR analysis of *H. lobatus* ZnO Nanoparticles

TheZnO NPs were synthesized via biomimetic methods through molecular interactions with metallic surfaces. The functional groups' interactions in the formulated materials were characterized using Fourier-transform infrared spectroscopy (FTIR). The FTIR spectrum of *H. lobatus* leaf ZnO nanoparticles (Figure 06) from 3565 cm^{-1} (medium, Sharp O-H stretching, alcohol), 3447 cm^{-1} (Strong, broad O-H stretching, aldehyde), 2851 cm^{-1} (strong, broad O-H stretching, carboxylic acid), 2764 cm^{-1} (weak, broad O-H stretching, alcohol), 2095 cm^{-1}

(strong, broad N=C=S stretching, amine salt), 2764 cm^{-1} (weak, broad O-H stretching, alcohol), 2093 cm^{-1} (strong N=C=S stretching, isothiocyanate), 1788 cm^{-1} (strongC=O stretching, acid halide), 1341 cm^{-1} (medium-H bending, alcohol), 1046 cm^{-1} (strongC-F stretching, fluoro compound), 835 cm^{-1} (medium C=C bending, alkene), and 752 cm^{-1} (strong C=C bending, alkene). 609cm^{-1} (strong, C-Cl stretching, halo compounds) and 504cm^{-1} (Strong, C-I stretching, Halo compounds). These peaks indicated significant bio-reduction and were similar to findings reported by [37,38] with minor shifts in peak positions. (Table 03) shows the compound classes present in functional groups.

Table 03. Showing compound class through FTIR

Wave Numbers	Group	Compound Class	Peak details
3565.31	O-H stretching	alcohol	Medium, sharp
3447.64	O-H stretching	alcohol	strong, broad
2851.92	O-H stretching	carboxylic acid	strong, broad
2764.43	O-H stretching	alcohol	weak, broad
2095.871	N=C=S stretching	isothiocyanate	strong
1788.84	C=O stretching	acid halide	strong
1341.96	O-H bending	alcohol	medium
1046.58	C-F stretching	fluoro compound	strong
835.92	C=C bending	alkene	medium
725.42	C=C bending	alkene	strong
609.66	C-Cl stretching	halo compound	strong
504.45	C-I stretching	halo compound	strong

3.3.3 SEM analysis of *H. lobatus* ZnO Nanoparticles.

SEM analysis of ZnO nanoparticles made with *Hibiscus lobatus* extract showed a varied array of nanostructures. The micrographs (Figure 07) revealed both individual spherical nanoparticles and clusters, averaging around 40 nm in size. These clusters likely form due to interparticle interactions like Van der Waals forces and hydrogen bonds, which are common in green-synthesized nanomaterials because of residual phytochemicals acting as capping agents. The observed spherical shape matches previous studies on green-synthesized ZnO nanoparticles. For example, [39]. described similar spherical ZnO nanostructures created via wet chemical methods, with sizes between 39.8 and 43 nm, showing smooth surfaces and moderate agglomeration due to plant-derived metabolites stabilizing the particles. The aspect ratio of the nanoparticles varies with temperature, with lower synthesis temperatures producing more uniform spherical particles with higher aspect ratios. Higher temperatures cause morphological changes, leading to coarser surfaces and lower aspect ratios. This pattern agrees with [40], who found that increasing temperature during ZnO synthesis with *Hibiscus subdariffa* extracts promotes particle growth and fusion, changing surface features and decreasing shape anisotropy. The tendency for agglomeration seen in the SEM images is typical for biosynthesized ZnO nanoparticles and is influenced by phytochemicals in *Hibiscus lobatus.* These biomolecules not only reduce metal ions but also regulate nucleation and growth, resulting in spherical nanocrystals with a relatively narrow size range.

3.3.4 EDX analysis of *H. lobatus* ZnO NPs

Further elemental analysis of the zinc oxide nanoparticles using the EDX spectrum (Figure 08) revealed distinct signals exclusively corresponding to zinc and oxygen, affirming the successful synthesis of ZnO nanoparticles. The absence of additional elemental peaks indicated high purity of the biosynthesized nanoparticles. The stoichiometric mass proportions of zinc and oxygen were also determined from the spectrumto be 41.8% and 38.4%, and the analysis of uncertainty is 12.32%**.** Respectively. As reported, in the case of *Hibiscus rosa sinensis* ZnO nanoparticles, it shows the EDX mass percentage of Zn is 52.08% and O is 47.92%, highlighting slight variations in elemental composition due to differences in synthesis conditions and precursor concentrations [41], the structural reliability of the synthesized ZnO nanoparticles was validated through X-ray diffraction (XRD) analysis, which confirmed their wurtzite crystalline phase, consistent with standard ZnO nanoparticle characteristics. The morphological assessment via scanning electron microscopy (SEM) revealed a uniform spherical shape, further supporting their high stability and homogeneity [42].

3.3.5 XRD analysis of *H. lobatus* ZnO NPs

The *H. lobatus* ZnO NPs were characterized using Cu Kα X-ray diffraction (XRD) to confirm the presence of Zinc and determine the material's crystal structure. The characteristic pattern, visible across 2θ values from approximately 31◦ to 68◦ (as illustrated in a figure), confirmed the formation of pure ZnO. Specific diffraction peaks were identified at 2θ values of 31.84◦, 34.49◦, 36.32◦, 47.62◦, 56.68◦, 62.93◦, and 68.03◦. These peaks correspond to the crystal planes (100), (002), (101), (102), (110), (103), (200), and (112), which is consistent with the reflection patterns previously reported for ZnO nanoparticles synthesized using *Artemisia absinthium* leaf extract (43). Similarly, observed peaks at 31.45◦, 34.66◦, 36.26◦, 47.48◦, 56.29◦, 62.7◦, and 68.31◦ also align with reflections from these same planes, mirroring results seen in ZnO NPs derived from *Limonium pruinosum* leaf extract [44]. The absence of extraneous peaks in the XRD spectrum confirms the high purity of the synthesized nanoparticles, demonstrating their suitability for a range of biomedical, environmental, and industrial applications. Calculation of the crystallite size using the Scherrer equation confirmed the material's nanoscale dimensions, a property that is expected to enhance their surface reactivity and functional efficiency. Collectively, these results affirm the value of plant-mediated ZnO nanoparticle synthesis as a robust and environmentally sustainable approach for developing nanomaterials.

3.3.6 ZETA and DLS analysis of *H. lobatus* ZnO nanoparticles

ZnO Nanoparticles synthesized through a green approach utilizing *Hibiscus lobatus* leaf extract were suspended in an aqueous colloidal medium at ambient conditions. Zeta potential analysis yielded a value of +6.6 mV (Figure 10A), signifying moderate electrostatic stabilization. The positive surface charge indicates the presence of repulsive interparticle forces, which suppress aggregation and enhance colloidal uniformity. This surface potential suggests efficient capping and stabilization, likely facilitated by phytoconstituents from the plant extract. Such electrostatic repulsion plays a crucial role in preserving nanoparticle dispersion by counteracting van der Waals attractions. Additionally, dynamic light scattering (DLS) was employed to assess the hydrodynamic size and distribution profile of the ZnO NPs, providing insights into their dispersibility and stability within the colloidal system. The values reported by [45] ranged between 20 and 130 nm. However, the *H. lobatus*-mediated exhibited a mean hydrodynamic size of approximately 145.2 nm (Figure 10B), which may be attributed to biomolecular surface interactions and possible nanoparticle agglomeration under colloidal conditions.

Similar observations were reported in studies on microbial-mediated ZnO NPs, where biological capping agents influenced nanoparticle size and dispersion [46]. The moderate zeta potential and increased hydrodynamic size suggest that the biosynthesized NPsmaintain reasonable stability in aqueous suspension, making them suitable for biomedical, environmental, and catalytic applications. The findings reinforce the importance of green synthesis approaches in producing ZnO NPswith enhanced biocompatibility and functional properties [47].

3.3.7 TEM analysis of *H. lobatus* ZnO nanoparticles

Transmission Electron Microscopy (TEM) was utilized to investigate the structural characteristics, particle size distribution, and spatial arrangement of zinc oxide nanoparticles synthesized via *Hibiscus lobatus* extract. As shown in Figures 11(a) and 11(b), both low- and high-resolution TEM micrographs reveal that the nanoparticles are spherical in predominantly with a high degree of size uniformity. The average particle diameter was approximately 10 nm, indicating the efficacy of the biosynthetic method in generating nanoscale materials. These findings are compatible with prior studies demonstrating that plant- and marine-derived extracts mediate nanoparticle synthesis through phytochemicals acting as reducing and capping agents [48]. The morphological uniformity observed suggests that bioactive constituents in the *H. lobatus* extract played a pivotal role in directing nucleation and regulating nanoparticle growth. A slight disparity between the particle size determined by TEM and the crystallite size obtained from X-ray Diffraction (XRD) analysis is attributed to the distinct measurement principles of the techniques, while XRD estimates the size of coherent diffracting crystalline domains, TEM offers direct visualization of the entire nanoparticle structure, including polycrystalline assemblies and organic surface coatings [49]. The well-defined grain boundaries and uniform image contrast observed in TEM further confirm the crystalline integrity and morphological stability of the synthesized ZnO nanoparticles**.** Confirm the crystalline quality of the nanoparticles. These characteristics are important in applications where surface properties, stability, and particle uniformity are critical, such as antimicrobial materials, photocatalysis, and nanomedicine delivery systems [50], the TEM findings support the efficacy of *H. lobatus*-assisted green synthesis as a sustainable route for producing Zinc Oxide nanoparticles with a preferred structure and functional properties, suitable for a scale of nanotechnological applications.

3.4 Anti-bacterial activity of *H. lobatus* ZnO nanoparticles

ZnO nanoparticles show an enhanced antibacterial activity against the tested pathogens, *Staphylococcus aureus* (*S.aureus*) and *Pseudomonas aeruginosa(P.aeruginosa*). (Figure 12). The strongest inhibition zone for an antibacterial effect was observed against *P. aeruginosa*, with inhibition zones measuring 17 mm and 20 mm at different concentrations of 1,2 and 3µg ZnO NP suspensions, respectively. Conversely, lower activity was noted against *S. aureus*, with inhibition zones of 16 mm and 20 mm at different concentrations, as shown in Table 04. Overall, NPsexhibited moderate antimicrobial efficacy. Studies, such as those by [51] indicate that the antibacterial action of ZnO NPs is ascribed to the disruption of the proton motive force and the internalization of toxic dissolved zinc ions. This process weakens the structural integrity of mitochondria, leads to intracellular membrane leakage, and activates oxidative stress-related gene expression. Such effects culminate in the inhibition of cell growth and eventual cell death, as corroborated by earlier findings from [52].

Table. 04: Antibacterial activity of H. lobatus ZnO Nps

Sl.	Sample Name	Conc. (µg)	*S. aureus*	*P. aeruginosa*
1	*H. lobatus* ZnO NPs	1	15.66 ± 0.57	15.33 ± 0.57
		2	16.66 ± 1.15	17.33 ± 0.57
		3	20.33 ± 0.57	20.33 ± 0.57
2	**Std./ Kanamycin**	10	6.66 ± 1.15	7.66 ± 0.57
		20	12.66 ± 0.57	13.33 ± 1.15
		30	14.33 ± 0.57	15.66 ± 0.57
		40	16.33 ± 0.57	18.66 ± 0.57

3.5 Antifungal activity of *H. lobatus* ZnO NPs

The antifungal activity of ZnO nanoparticles synthesized from Aqueous *Hibiscus lobatus* leaf extract was assessed against *Aspergillus avus* and *Pichia anomala* using the well diffusion method. As depicted in (Figure 13), the ZnO NPs exhibited a pronounced inhibitory effect on *A. flavus*, with inhibition zone diameters of 7 mm, 9 mm, and 14 mm at concentrations of 200, 300, and 400 µg/mL, respectively, as shown in (Table 05), highlighting a clear dose-dependent trend. These results are consistent with prior findings reported by [53] who also observed concentration-dependent antifungal efficacy of ZnO NPs. In contrast, the nanoparticles demonstrated comparatively lower inhibition against *P. anomala*, with zones of 8 mm and 13 mm observed at similar concentrations. This disparity in antifungal response between the two fungal strains suggests that nanoparticle-cell membrane interactions differ depending on fungal species, influencing their susceptibility. Similar trends were noted by [54] who reported enhanced inhibition of *Aspergillus* species by ZnO NPs, particularly *A. flavus*, under escalating concentrations. The antifungal mechanism of action is largely attributed to the nanoparticles' ability to generate reactive oxygen species (ROS), which impose oxidative stress on fungal cells, disrupting cellular metabolism and impairing viability (55) Collectively, these findings support the notion that the physicochemical characteristics of *H. lobatus*-mediated ZnO NPs, especially their ROS-generating potential, underpin their selective yet promising antifungal behaviour.

Table 05: Antifungal activity of in the zone of inhibition (mm)

Sl.	Sample Names	Conc. (µg)	*A. flavors*	*P. anomala*
1	***H. lobatus* ZnO NPs**	100	---	---
		200	---	7.33 ± 0.57
		300	8.33± 1.15	9.33± 0.57
		400	13.33± 0.57	14.66± 0.57
2	**Standard/ Fluconazole**	20	---	---
		40	---	---
		60	13.33 ± 0.57	14.66 ± 0.57
		80	16.33 ± 0.57	20.33 ± 1.15

Note: - '---' indicates no activity shown at the tested concentrations

3.6 Antioxidant activity by DPPH assay of *H. lobatus* ZnO NPs

The DPPH assay of biosynthesized H*. lobatus.* Scavenging activity was detected in various concentrations from 0,50,100, and 150,200,250 mg/mL, where the inhibition ratios were 11, 30, 52, 74, 92, respectively. The ZnO NPs demonstrated a significant, dose-dependent increase in scavenging potency by donating electrons to neutralize the DPPH free radicals. Notably, their activity surpassed that of the positive control, ascorbic acid (23.55 µg/mL). The DPPH radical scavenging activity was clearly exhibited by the biosynthesized ZnO nanoparticles.

(ZnO NPs) *H. lobatus* demonstrates a significant dose-dependent antioxidant effect (Table 06). The inhibition ratios observed at concentrations ranging from 50 to 250 mg/mL indicate a progressive increase in scavenging potency, with the highest inhibition reaching 92% at 250 mg/mL. This shows the ZnO NPs effectively neutralize DPPH free radicals by transferring electrons, thereby reducing oxidative stress. Interestingly, the antioxidant activity of *H. lobatus* ZnO NPs surpasses that of ascorbic acid (23.55 µg/mL, positive control) (Figure 14), reinforcing their potential as a strong antioxidant agent. The occurrence of phenolic and flavonoid compounds in the Zinc oxide NPs likely enhances their radical scavenging ability, as these phytochemicals are well-documented for their antioxidant properties. Correlating with these findings with previous studies, ZnO NPs synthesized *using Luffa acutangula exhibited* an IC_{50} value of 134 µg/mL (56), *whereas H. lobatus* ZnO NPs demonstrated a slightly higher IC_{50} value of 145 µg/mL (Figure 15). This difference suggests that the biological source of ZnO NPs plays a crucial role in determining their antioxidant efficacy. The observed variation in IC_{50} values can be attributed to several factors, including differences in nanoparticle size, surface charge, and the presence of bioactive phytochemicals, all of which critically influence their interactions with free radicals. Recent investigations have highlighted the potent antioxidant properties of ZnO nanoparticles synthesized through diverse biological routes. Notably, Ag-ZnO composite nanoparticles produced via green synthesis methods have demonstrated enhanced radical-scavenging activity, owing to the synergistic effects between zinc oxide and silver, the phytoconstituents involved in the synthesis process. *Capparis zeylanica* leaf extract exhibited a DPPH scavenging activity value of 340 µg/mL, which is higher than that of ascorbic acid (289.74 µg/mL). (57) ZnO NPs synthesized using *Phoenix dactylifera L.* polyphenols demonstrated enhanced total antioxidant capacity (TAC) and DPPH scavenging activity, reinforcing their role in oxidative stress reduction [58]. These findings suggest that the biological source of Zinc oxide NPS plays a crucial role in determining their antioxidant efficacy. The presence of phenolic and flavonoid compounds in plant extracts enhances the radical scavenging ability of Zinc oxide nanoparticles, making them promising candidates for biomedical and environmental applications.

Table 06: Antioxidant activity by DPPH assay of ZnO Nps

Sl No	Sample Name	DPPH IC_{50}(µg/ml)
1	**Vit-C**	23.55± 1.86
2	***H. lobatus*ZnO NPs**	145.80 ± 9.81

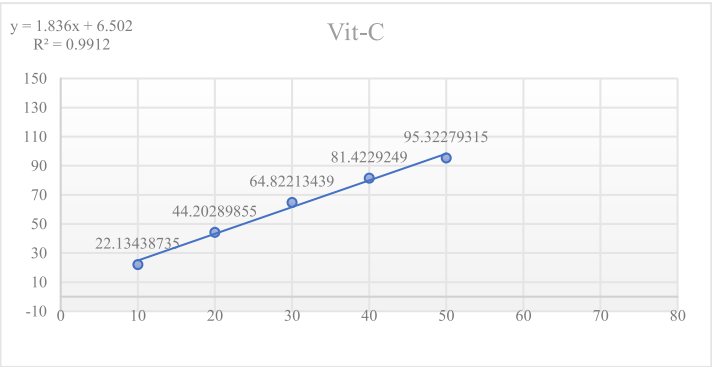

Figure 14: showing the antioxidant activity of vitamin C taken as a standard

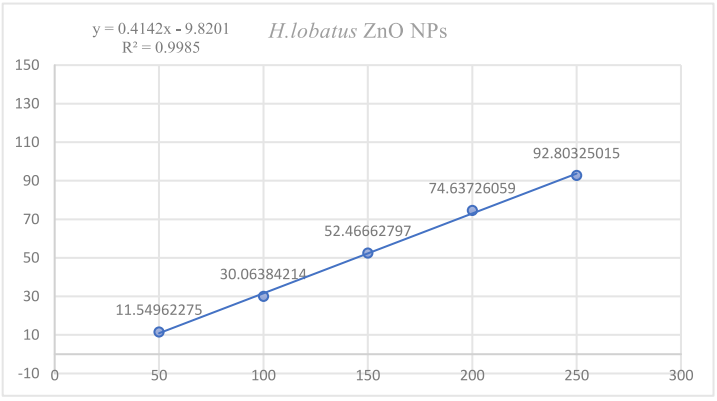

Figure 15: showing antioxidant activity of H. lobatus. ZnO NPs (Rc2)

3.7 Antidiabetic activity by α-Glucosidase inhibition

The synthesized *H. lobatus.*ZnO NPs (RC2) describes a concentration-dependent inhibition, with percentages of 5%, 14%, 29%, 47%, and 62% at concentrations of 20µL, 40µL, 60µL, 80µL, and 100µL, respectively. The IC_{50} value is 62.14µg/ml (Figure 17), as shown in Table 07, as the standard acarbose showed percentages ranging from 13% to 86% at the corresponding concentrations. Its standard value (Acarbose) is 29.51µg/ml. (Figure 16) These results show the capacity of ZnO NPs in modulating α-glucosidase activity, with the herbal formulation influencing their inhibitory effects. Using*T. Indica* (ZnO-S6) exhibited higher α-glucosidase inhibition activity in the report (Rehana et *al.,*2017). The research on *Tamarindus indica*-derived ZnO nanoparticles (ZnO-S6) has demonstrated enhanced α-glucosidase inhibition, reinforcing the effectiveness of plant-mediated ZnO NPs in antidiabetic applications [59]. Further studies, such as those by (60), have explored the Optimization and Analysis of green-synthesized ZnO Nanoparticles, confirming their strong suppressive potential against. The material demonstrated inhibitory effects against α-amylase and α-glucosidase, with IC_{50} values determined to be 103.20±1.03 µg/mL and 94.14±0.37 µg/mL, respectively [61]. These results show that the plant-mediated ZnO NPs could serve as effective hypoglycemic agents, contributing to diabetes treatment strategies.

Table. 07: α-Glucosidase inhibition activity

Sl. No.	Samples	α-Glucosidase inhibition (IC_{50} µg/ml)
1	**Acarbose/Std.**	29.51± 2.04
2	***H. lobatus*. ZnO NPs**	62.14± 3.04

Note: - '---' indicates no activity shown at the tested concentrations

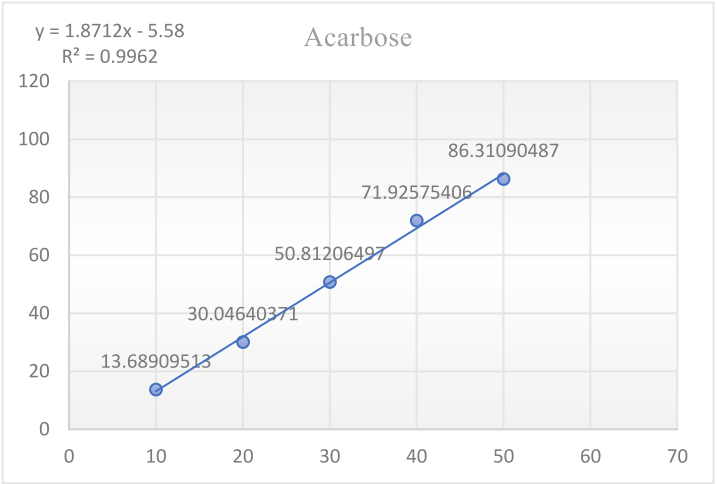

Figure 16: showing the anti-diabetic activity of Acarbose taken as a standard

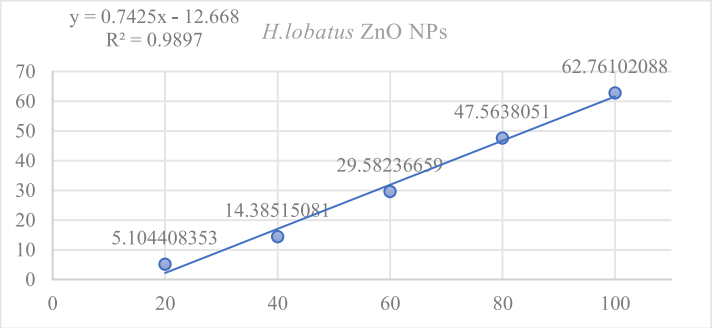

Figure 17: showing an α-Glucosidase inhibition assay. Lobatus ZnO NPs (Rc2)

3.8 Evaluation of cytotoxicity effects from *H. lobatus.* ZnO NPs

The ZnO NPs of *H. lobatus* exhibited a concentration-dependent inhibition for the MCF7 and A549 (Figure 20 & Figure 21) cancer cell lines with concentrations of 5, 25, 100, 250, and 500µg/ml, respectively (Figure 18 & Figure 19). The IC_{50} value of *H. lobatus* ZnO NPs for MCF7 and A549 is 101.9µg/ml and 84.11 µg/ml, respectively, as presented in (Table 08). Similar results were seen in *Fioria vitifolia* plant-mediated ZnO NPs, which showed toxicity levels of 86.6 µg/ml and 88.6 µg/ml, indicating a rise in toxicity effects due to morphological changes and cell death at high densities, attributed to the high surface area and size of the nanoparticles [62]. As the standard, Doxorubicin showed from 1% to 98% at the corresponding concentrations. These results indicate the potential of ZnO NPs in modulating cytotoxicity activity, with the herbal formulation influencing their effects. Using *A. indicum* extract of ZnO NPs exhibited cytotoxicity effect A549 cancer cell line, exhibiting a similar IC_{50} value of 29 ± 0.5 µg/ml in the report [63]. Further studies, such as those by [64], have explored the cytotoxicity of ZnO nanoparticles on MCF-7 cells, demonstrating that nano-sized ZnO (20–30 nm) exhibited enhanced toxicity when dispersed in phosphate-buffered saline, compared to media containing 10% fetal bovine serum, due to the absence of protein protection. Additionally, a meta-analysis by [65] confirmed that ZnO NPs, along with Ag and Au nanoparticles, exhibited significant cytotoxicity at concentrations ≥60 µg/mL, reinforcing their role in nanomedicine-based cancer therapy. These findings highlight the potential of ZnO NPs as effective anticancer agents, capable of selectively targeting malignant tumor cells while reducing damage to healthy tissues. Their high surface reactivity, oxidative stress induction, and apoptotic effects make plant-mediated ZnO NPs promising candidates for nanoparticle-based cancer treatments, as shown in (Figures 20 & and 21).

Table. 08: cytotoxicity effect from H. lobatus. ZnO NPs through MCF7 and A549 Cancer cell lines

Sl. No.	Samples	MCF7 Cancer cell line (IC_{50} µg/ml)	A549 cancer cell line (IC_{50} µg/ml)
1	***H. lobatus***	101.9 µg/ml	84.11 µg/ml
2	**Std (Doxorubicin)**	45.17µg/ml	46.36µg/ml

Note: - '---' indicates no activity shown at the tested concentrations

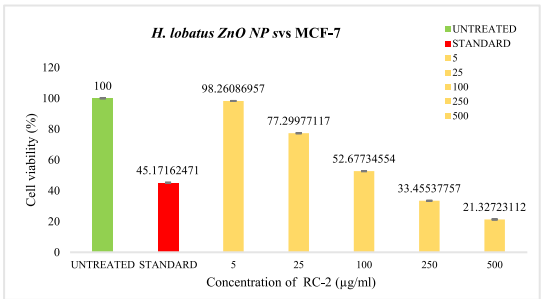

Figure 18: Showing the cytotoxic effects of the H. lobatus ZnO NPs on the MCF-7 cell line

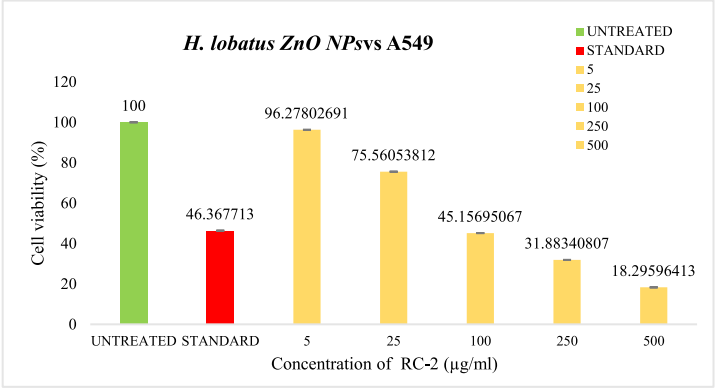

Figure 19: Showing the cytotoxic effects of the H. lobatus ZnO NPs on the A549 cell line

4. CONCLUSION

The Green synthesis of Zinc Oxide nanoparticles. This was achieved using an aqueous leaf extract of *Hibiscus lobatus*, employing green chemistry principles to ensure an eco-friendly, rapid, non-toxic, and cost-effective approach. The bio-synthesized ZnO NPs show a distinct absorption peak at 374 nm, as confirmed by UV-Vis, indicating successful nanoparticle formation. FTIR analysis revealed the presence of biological functional groups responsible for reduction, capping, and stabilization, ensuring nanoparticle integrity. The XRD analysis validated the crystalline nature of ZnO nanoparticles, with Bragg's planes confirming their structural formation. The nanoparticles displayed a spherical morphology, and their sizes varied from 8.8 nm to 27.76 nm, a range that supports optimal surface reactivity. To assess long-term stability, the Zeta potential was measured, demonstrating the colloidal stability of ZnO NPs.The antimicrobial efficacy of Zinc oxide NPs was evaluated against human pathogens, showcasing potent antibacterial and antifungal activity. Additionally, their antioxidant potential was confirmed, highlighting their ability to neutralize free radicals and mitigate oxidative stress. The *in-vitro* anti-diabetic assessment demonstrated their role in glucose regulation, contributing to the maintenance of blood sugar levels. Furthermore, their anti-cancer properties exhibited consistent cytotoxic effects, reinforcing their potential as therapeutic agents. These findings suggest that *H. lobatus*-derived ZnO NPscould serve as biocompatible nanomaterials for pharmaceutical, agricultural, and biomedical applications. Their low toxicity, high biological activity, and multifunctional properties make them promising for nanomedicine and pathogen control, pending further validation through clinical trials.

ACKNOWLEDGEMENT

The authors gratefully acknowledge the P.G. Department of Studies in Botany, Davangere University, Davangere. I also thank my research supervisor for providing lab facilities to conduct the experiments. The authors also thank Dr. Sudarshan B.L. Cheliyan of the Biotech Laboratory, Mysore. And the University Scientific Instrumentation Centre (USIC), Karnatak University, Dharwad, for their essential instrumentation services.

CONFLICT OF INTEREST

The authors declare that there is no conflict of interest regarding the publication of this manuscript.

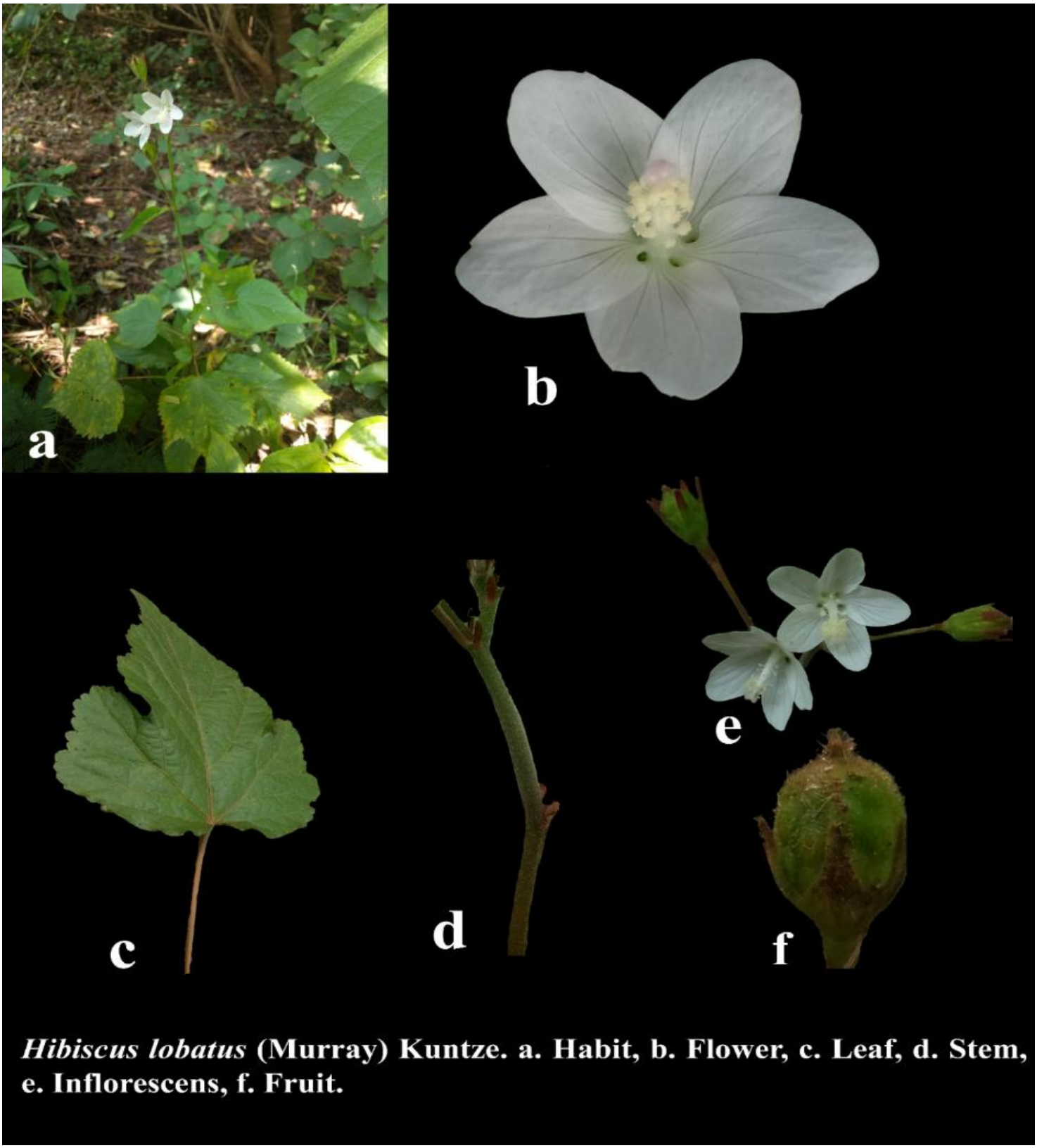

Figure. 01. Hibiscus lobatus plant

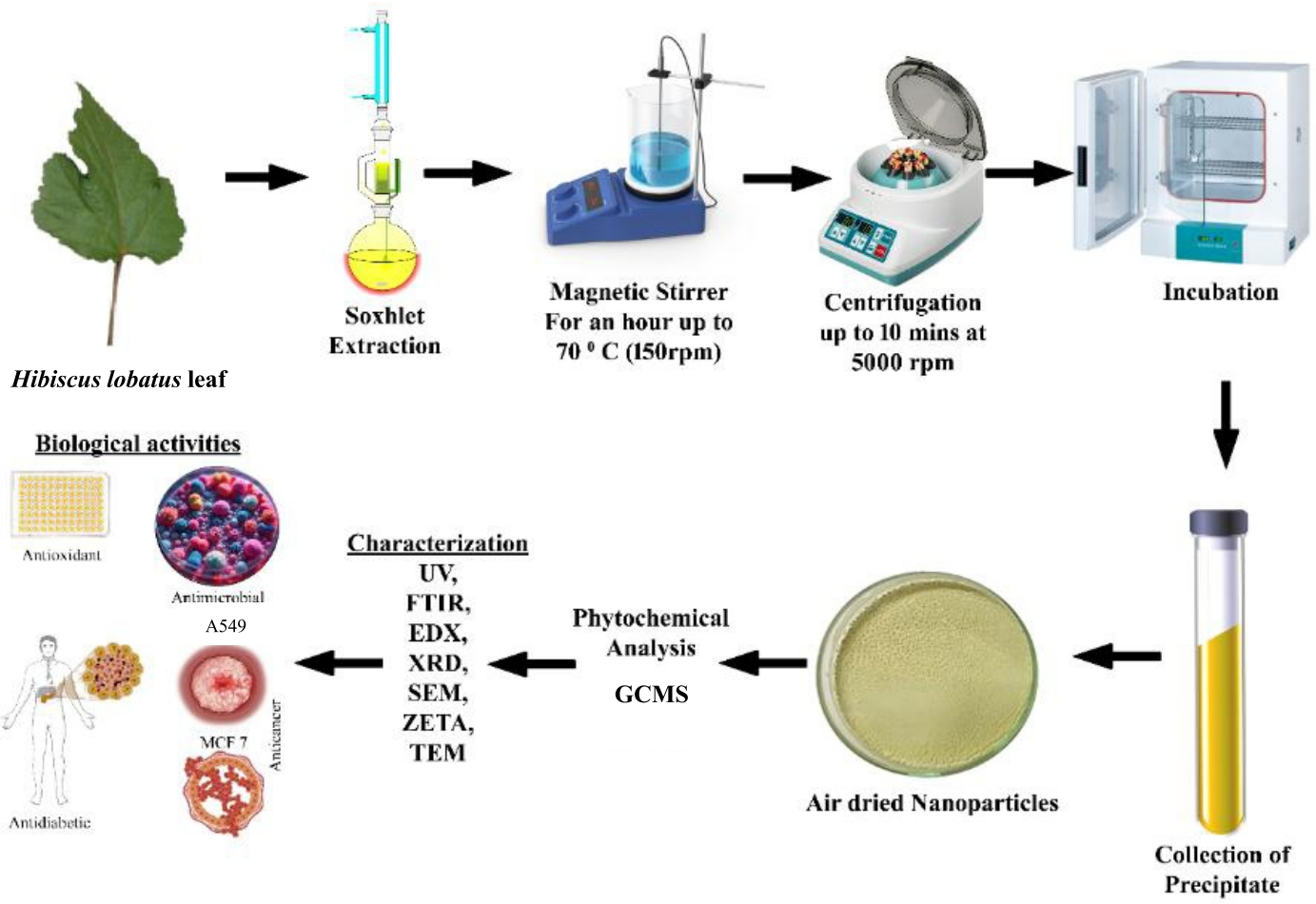

Figure.02: Preparation of H. lobatusPlant leaf extract, synthesis, characterization and biological activity

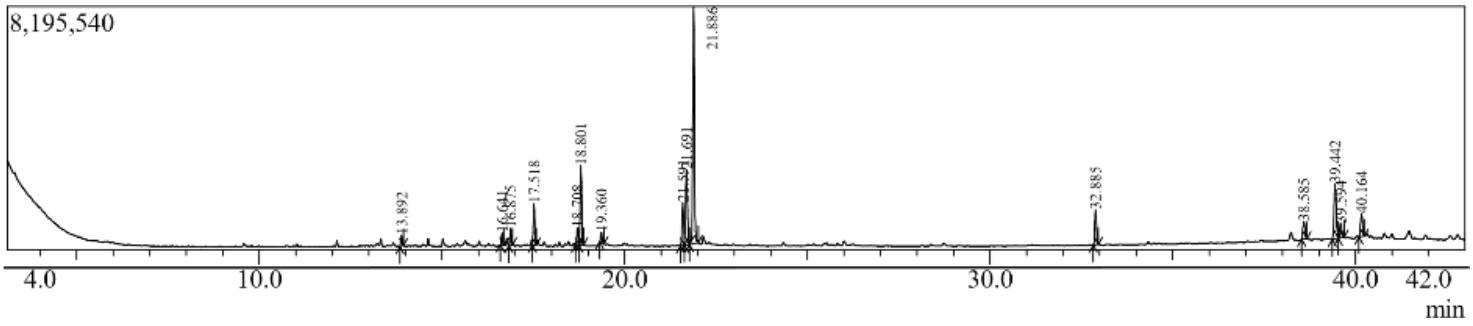

Figure. 03: Showing a GC-MS Chromatogram of Hibiscus lobatusAq.plant leaf extract

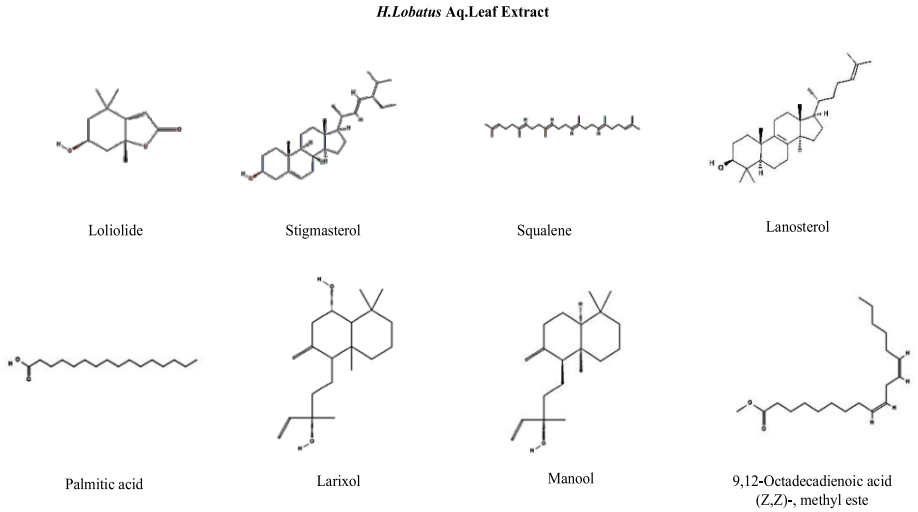

Figure. 04. CompoundAnalysis of H. lobatus leaf extract by GC-MS

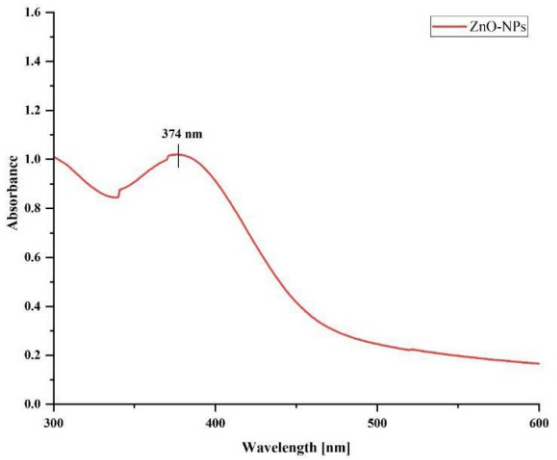

Figure. 05. Visual and UV–Vi's analysis ofH. lobatusZnO Nps

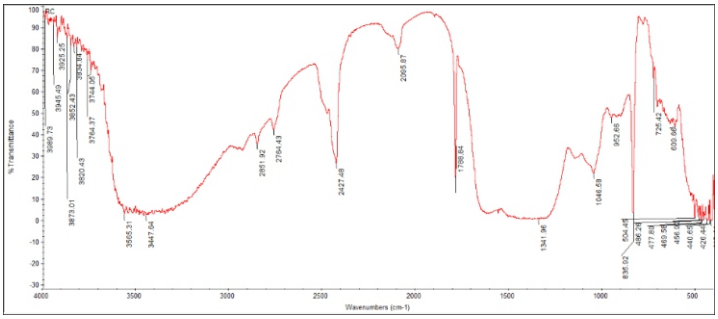

Figure. 06. FTIR analysis of H. lobatus ZnO Nps

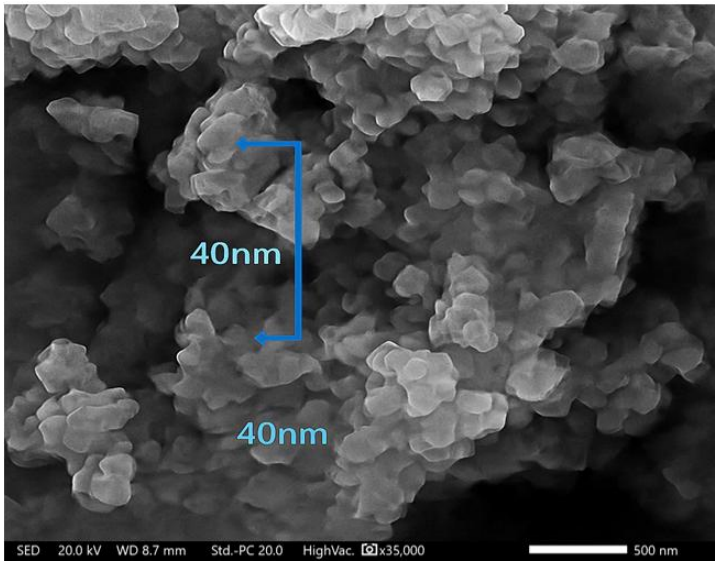

Figure. 07. SEM analysis of H. lobatus ZnO Nps

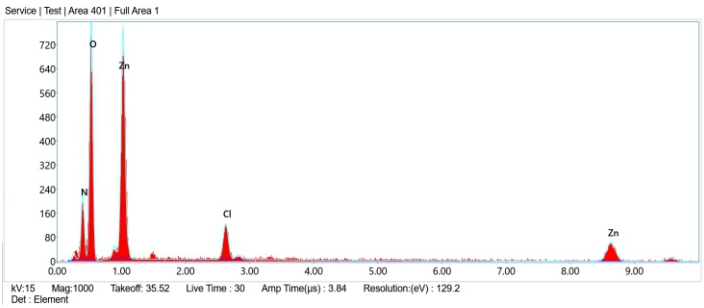

Figure. 08. EDX analysis of ZnO Nps

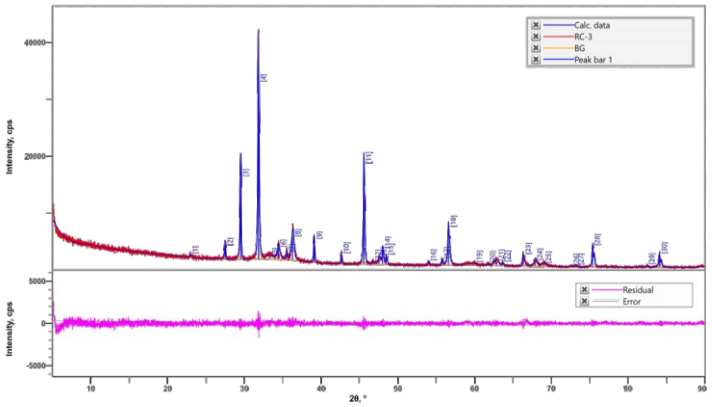

Figure. 09. XRD analysis of ZnO Nps

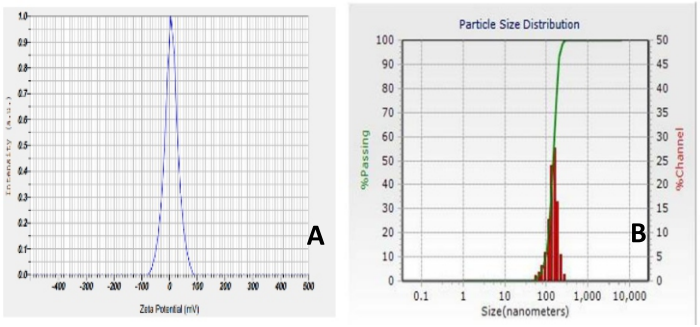

BFigure. 10. A) Zeta potential and B) DLS analysis of ZnO Nps.

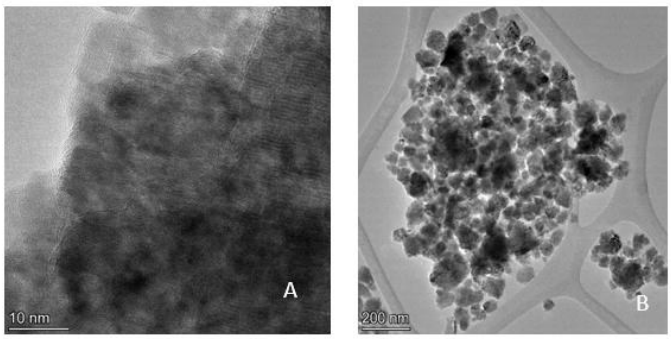

Figure 11: Transmission electron microscope images of zinc oxide nanoparticles recorded at (a) low & (b) high magnifications

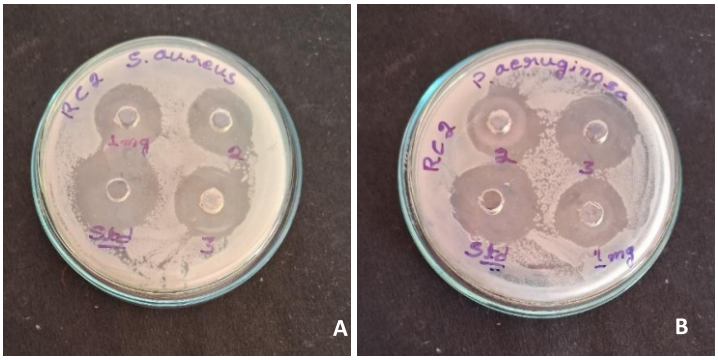

Figure. 12. Antibacterial activity of H. lobatus ZnO NPs; A) S.aureus B) P. aeruginosa

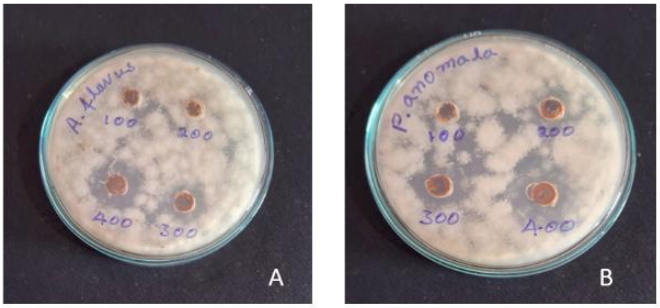

Figure 13. Antifungal activity of H. lobatus ZnO NPs; A) A. flavus, B) P. anomala

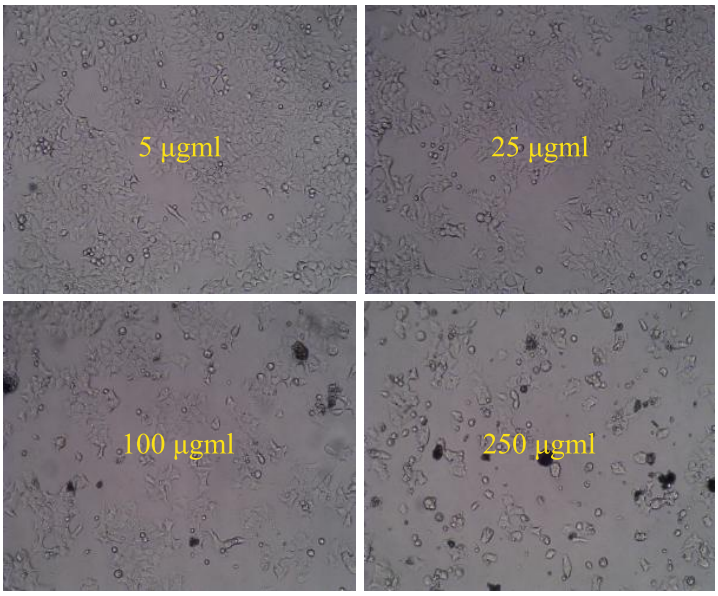

Figure. 20: showing a H. lobatus ZnO NPsagainst MCF-7 cancer cell line

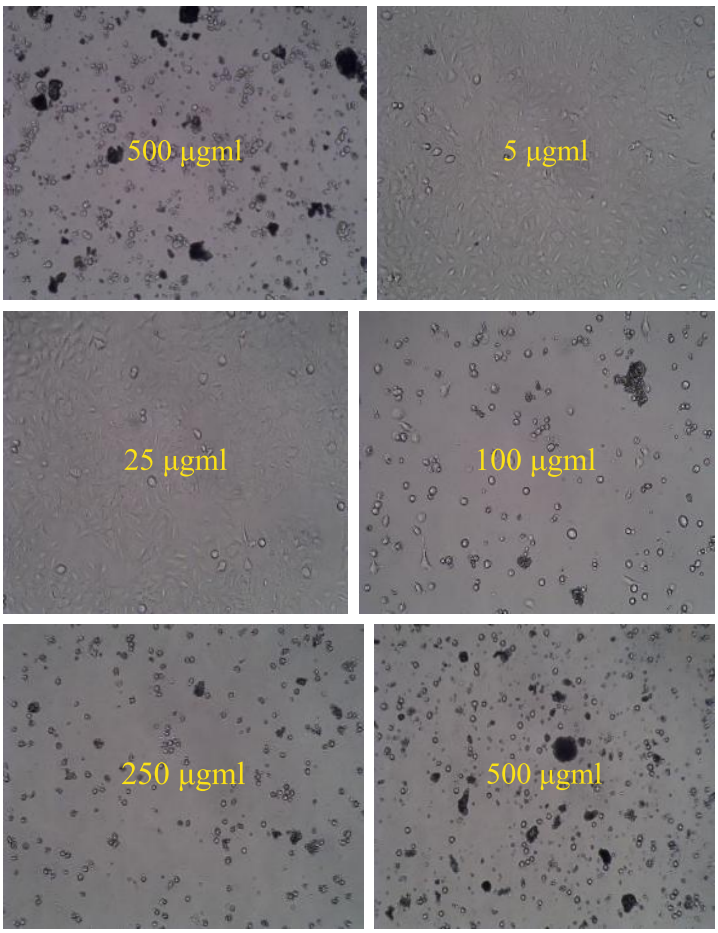

Figure 21: showing H. lobatus ZnO NPsagainst the A549 cancer cell lin

References

1. Sivarajan, V. V., & Pradeep, A. K. (1996). *Malvaceae of southern peninsular India: a taxonomic monograph*. Daya Books.

2. Erarslan, Z. B., & Koçyiğit, M. (2019). The important taxonomic characteristics of the family Malvaceae and the herbarium specimens in ISTE. *Turkish Journal of Bioscience and Collections*, *3*(1), 1-7.

3. Rahman, A. H. M. M., & Gondha, R. (2014). Taxonomy and Traditional Medicine Practices on Malvaceae (Mallow Family) of Rajshahi, Bangladesh. *Open Journal of Botany*, *1*(2), 19-24.

4. Dhuha Sabah Nadir, & Alhan mohammedalwan. (2022). Medical Properties of *Abutilon hirtum* (Lam.) Sweet (Malvaceae): A Review. *Eurasian Medical Research Periodical*, *14*, 35–43.

5. Rakshit, S. C., & Kundu, B. C. (1970). Revision of the Indian species of Hibiscus. *Nelumbo*, 151-175.

6. Tyagi, S., & Pandey, V. K. (2016). Research & Reviews: Journal of Pharmaceutics and Nanotechnology. *JPN*, *4*, 2-12.

7. Mondal, S.K., Chakraborty, S., Manna, S., & Mandal, S. M. (2024). Antimicrobial nanoparticles: current landscape and future challenges. *RSC Pharmaceutics*, *1*(3), 388-402.

8. Parveen K, Banse V, Ledwani L. Green synthesis of nanoparticles: Their advantages and disadvantages. In AIP conference proceedings 2016 Apr 13 (Vol. 1724, No. 1). AIP Publishing.

9. Khalil, I., Yehye, W. A., Etxeberria, A. E., Alhadi, A. A., Dezfooli, S. M., Julkapli, N. B. M., ... &Seyfoddin, A. (2019). Nanoantioxidants: Recent trends in antioxidant delivery applications. *Antioxidants*, *9*(1), 24.

10. Fallah, S., Yusefi-Tanha, E., & Peralta-Videa, J. R. (2024). Interaction of nanoparticles and reactive oxygen species and their impact on macromolecules and plant production. *Plant Nano Biology*, 100105.

11. Abd El-Megeed, S., & El-Sayed, W. (2022). The potential role of zinc oxide nanoparticles in the treatment of diabetes mellitus: an updated review. *Zagazig Veterinary Journal*, *50*(1), 37-51.

12. Yousaf, I. (2024). The Current and Future Perspectives of Zinc Oxide Nanoparticles in the Treatment of Diabetes Mellitus. *arXiv preprint arXiv:2409.04486*.

13. Amiri, A., Dehkordi, R. A. F., Heidarnejad, M. S., &Dehkordi, M. J. (2018). Effect of the zinc oxide nanoparticles and thiamine for the management of diabetes in alloxan-induced mice: a stereological and biochemical study. *Biological trace element research*, *181*, 258-264.

14. Bisht, G., & Rayamajhi, S. (2016). ZnO nanoparticles: a promising anticancer agent. *Nanobiomedicine*, *3*, 9.

15. Camarillo, I. G., Xiao, F., Madhivanan, S., Salameh, T., Nichols, M., Reece, L. M., ... & Sundararajan, R. (2014). Low and high voltage electrochemotherapy for breast cancer: An in vitro model study. *Electroporation-based therapies for cancer*, 55-102.

16. Sundararajan, R., Salameh, T., Camarillo, I. G., Prabu, R. R., Natarajan, A., & Sankaranarayanan, K. (2014). Irreversible electroporation: a drug-free cancer treatment. *Electroporation-Based Therapies for Cancer*, 219-243.

17. Harborne, J. B. (1973). Phytochemicals Methods. Chapman and Hall Ltd., London

18. Chakraborty, B., Raju, S.K., Abdulrahman, I.A., Karthikeyan, P., Sreenivasa, N., Kathirvel, B., 2022. Streptomyces filamentous strain KS17 isolated from microbiologically unexplored marine ecosystems exhibited a broad spectrum of antimicrobial activity against human pathogens. Process Biochem. 117, 42– 52. https://doi.org/10.1016/j.procbio.2022.03.010.

19. Yassin, M. T., Al-Askar, A. A., Maniah, K., & Al-Otibi, F. O. (2022). Green synthesis of zinc oxide nanocrystals utilizing *origanummajorana* leaf extract and their synergistic patterns with colistin against multidrug-resistant bacterial strains. *Crystals*, *12*(11), 1513.

20. Lahoti, R., & Carroll, D. (2025). Green synthesis of zinc oxide nanoparticles and their broad-spectrum antibacterial activity. *Next Research*, *2*(1), 100164

21. Darshan, R. C., &Kakkalameli, S. B. (2025). Phytochemical Screening, Proximate Analysis and Phyto-synthesis of Zinc Oxide Metallic Nanoparticles from the Leaf of *Abutilon persicum* (Burm. F.) Merr. and their Biological Applications. *Asian Journal of Applied Chemistry Research*, *16*(2), 173-200.

22. Daphedar, A. B., Kakkalameli, S. B., Melappa, G., Taranath, T. C., Srinivasa, C., Shivamallu, C., ... & Kollur, S. P. (2021). Genotoxic assay of silver and zinc oxide nanoparticles synthesized by leaf extract of Garcinia livingstonei T. Anderson: A comparative study. *Pharmacognosy Magazine*, *17*(05).

23. Akhter, S. M. H., Siddiqui, V. U., Ahmad, S., Husain, D., Naeem, S., & Alam, M. T. (2024). Sustainable synthesis of zinc oxide nanoparticles using Terminalia chebula extract: Effect of concentration and temperature on properties and antibacterial efficacy. *Nano-Structures & Nano-Objects*, *38*, 101158.

24. Perumal, P., Sathakkathulla, N. A., Kumaran, K., Ravikumar, R., Selvaraj, J. J., Nagendran, V., ... & Rathinasamy, S. (2024). Green synthesis of zinc oxide nanoparticles using aqueous extract of shilajit and their anticancer activity against HeLa cells. *Scientific Reports*, *14*(1), 2204.

25. Sreenivasa, N.; Bidhayak, C.; Pallavi, S.S.; Bhat, M.P.; Shashiraj, K.N.; Ghasti, B. Synthesis of Biogenic Silver Nanoparticles using *Zanthoxylum rhetsa* (Roxb.) DC Seed Coat Extract as Reducing Agent and In Vitro Assessment of Anticancer Effect on A549 Lung Cancer Cell Line. Int. J. Pharm. Res. 2020, 12, 302–314

26. Ranjitha, N., Krishnamurthy, G., Manjunatha, M. N., Naik, H. B., Pari, M., Vasantakumarnaik, N. K., ... & Pradeepa, K. (2023). Electrochemical determination of glucose and H2O2 using Co (II), Ni (II), Cu (II) complexes of novel 2-(1, 3-benzothiazol-2-ylamino)-N-(5-chloro-2-hydroxyphenyl) acetamide: Synthesis, structural characterization, antimicrobial, anticancer activity, and docking studies. Journal of Molecular Structure, 1274, 134483.

27. Blois, M. S. (1958). Antioxidant determinations by the use of a stable free radical. *Nature*, *181*(4617), 1199-1200

28. Poovitha, S., Parani, M. In vitro and in vivo α-amylase and α-glucosidase inhibiting activities of the protein extracts from two varieties of bitter gourd *(Momordica charantia*L.). BMC Complement Altern Med 16, 185 (2016). https://doi.org/10.1186/s12906-016-1085-1

29. Alley, M. C., Scudiere, D. A., Monks, A., Czerwinski, M., Shoemaker, R. II., and Boyd, M. R. Validation of an automated microculture tetrazolium assay (MTA) to assess growth and drug sensitivity of human tumor cell lines. Proc. Am. Assoc. Cancer Res., 27: 389, 1986

30. Mosmann T. Rapid colorimetric assay for cellular growth and survival: application to proliferation and cytotoxicity assays. J Immunol Methods. 1983; 65: 55–63.

31. Rassem, H., Nour, A. H., & Yunus, R. M. (2017). GC-MS analysis of bioactive constituents of Hibiscus flower. *Aust. J. Basic Appl. Sci*, *11*, 91-97.

32. Sehim, A. E., Amin, B. H., Yosri, M., Salama, H. M., Alkhalifah, D. H., Alwaili, M. A., & Abd Elghaffar, R. Y. (2023). GC-MS analysis, antibacterial, and anticancer activities of *Hibiscus sabdariffa* L. methanolic extract: In vitro and silico studies. *Microorganisms*, *11*(6), 1601.

33. SasaniGhamsari M, Alamdari S, Han W, Park HH. Impact of nanostructured thin ZnO film in ultraviolet protection. International journal of nanomedicine. 2017 Dec 28:207-16.

34. Talam, S., Karumuri, S. R., & Gunnam, N. (2012). Synthesis, characterization, and spectroscopic properties of ZnO nanoparticles. *International Scholarly Research Notices*, *2012*(1), 372505.

35. Selim, Y. A., Azb, M. A., Ragab, I., & HM Abd El-Azim, M. (2020). Green synthesis of zinc oxide nanoparticles using aqueous extract of *Deverratortuosa* and their cytotoxic activities. *Scientific reports*, *10*(1), 3445.

36. Kulkarni, S. S., &Shirsat, M. D. (2015). Optical and structural properties of zinc oxide nanoparticles. *Int. J. Adv. Res. Phys. Sci*, *2*(1), 14-18.

37. Karthik, L., Kumar, G., Kirthi, A. V., Rahuman, A. A., & Bhaskara Rao, K. V. (2014). Streptomyces sp. LK3-mediated synthesis of silver nanoparticles and its biomedical application. *Bioprocess and biosystems engineering*, *37*, 261-267.

38. Dutta, A. (2017). Fourier transforms infrared spectroscopy. *Spectroscopic methods for nanomaterials characterization*, 73-93.

39. Khan, S. B., Khan, M. I., & Nisar, J. (2022). Microwave-assisted green synthesis of pure and Mn-doped ZnO nanocomposites: In vitro antibacterial assay and photodegradation of methylene blue. *Frontiers in Materials*, *8*, 710155.

40. Bala, N., Saha, S., Chakraborty, M., Maiti, M., Das, S., Basu, R., & Nandy, P. (2015). Green synthesis of zinc oxide nanoparticles using *Hibiscus subdariffa* leaf extract: effect of temperature on synthesis, anti-bacterial activity and anti-diabetic activity. *RSC Advances*, *5*(7), 4993-5003.

41. Pavithra, S., Sudha, P., Kalaiselvi, V., Ramya, V., & Vidhya, N. (2020). Green Synthesis and Characterization of ZnO Nanoparticles using Hibiscus rosa-sinensis Leaf Extract. *J. Environ. Nanotechnol*, *9*(3), 07-12.

42. Maheswari, T. U. Anti-Inflammatory Effects and EDX Spectra Analysis of Zinc Oxide Nanoparticles Synthesized Using Phoenix dactylifera Extracts: An In Vitro Study. *Tuijin Jishu/Journal of Propulsion Technology*, *45*(3), 2024.

43. Alharbi, F. N., Abaker, Z. M., &Makawi, S. Z. A. (2023). Phytochemical substances—mediated synthesis of zinc oxide nanoparticles (ZnO NPs). *Inorganics*, *11*(8), 328.

44. Naiel, B., Fawzy, M., Halmy, M. W. A., & Mahmoud, A. E. D. (2022). Green synthesis of zinc oxide nanoparticles using *Sea Lavender* (Limonium pruinosum L. Chaz.) extract: characterization, evaluation of anti-skin cancer, antimicrobial and antioxidant potentials. *Scientific Reports*, *12*(1), 20370.

45. Gu, W., Li, H., Niu, X., & Zhou, J. (2022). The biological fabrication of ZnO nanoparticles from *Nepeta cataria* potentially produces apoptosis through the inhibition of proliferative markers in ovarian cancer. *Green Processing and Synthesis*, *11*(1), 316-326

46. Murali, M., Gowtham, H. G., Shilpa, N., Singh, S. B., Aiyaz, M., Sayyed, R. Z., ... &Kollur, S. P. (2023). Zinc oxide nanoparticles prepared through microbial mediated synthesis for therapeutic applications: a possible alternative for plants. *Frontiers in Microbiology*, *14*, 1227951.

47. Mohd Yusof, H., Mohamad, R., Zaidan, U. H., & Abdul Rahman, N. A. (2019). Microbial synthesis of zinc oxide nanoparticles and their potential application as an antimicrobial agent and a feed supplement in the animal industry: a review. *Journal of animal science and biotechnology*, *10*, 1-22.

48. Ahmad, H., Venugopal, K., Rajagopal, K., De Britto, S., Nandini, B., Pushpalatha, H. G., ... &Jogaiah, S. (2020). Green synthesis and characterization of zinc oxide nanoparticles using Eucalyptus globules and their fungicidal ability against pathogenic fungi of apple orchards. *Biomolecules*, *10*(3), 425.

49. Pu, Y., Niu, Y., Wang, Y., Liu, S., & Zhang, B. (2022). Statistical morphological identification of low-dimensional nanomaterials by using TEM. *Particuology*, *61*, 11-17.

50. Sirelkhatim, A., Mahmud, S., Seeni, A., Kaus, N. H. M., Ann, L. C., Bakhori, S. K. M., ... & Mohamad, D. (2015). Review on zinc oxide nanoparticles: antibacterial activity and toxicity mechanism. *Nano-micro letters*, *7*, 219-242.

51. Alaya, L., Saeedi, A. M., Alsaigh, A. A., Almalki, M. H., Alonizan, N. H., &Hjiri, M. (2023). ZnO: V nanoparticles with enhanced antimicrobial activities. *Journal of Composites Science*, *7*(5), 190.

52. Sirelkhatim, A., Mahmud, S., Seeni, A., Kaus, N. H. M., Ann, L. C., Bakhori, S. K. M., ... & Mohamad, D. (2015). Review on zinc oxide nanoparticles: antibacterial activity and toxicity mechanism. *Nano-micro letters*, *7*, 219-242.

53. Naiel, B., Fawzy, M., Halmy, M. W. A., & Mahmoud, A. E. D. (2022). Green synthesis of zinc oxide nanoparticles using *Sea Lavender* (Limonium pruinosum L. Chaz.) extract: characterization, evaluation of anti-skin cancer, antimicrobial and antioxidant potentials. *Scientific Reports*, *12*(1), 20370.

54. Achilonu, C. C., Kumar, P., Swart, H. C., Roos, W. D., & Marais, G. J. (2024). Zinc Oxide: Gold Nanoparticles (ZnO: Au NPs) Exhibited Antifungal Efficacy Against *Aspergillus niger* and *Aspergillus candidus*. *BioNanoScience*, *14*(2), 799-813.

55. Jasim, N. O. (2015). Antifungal activity of Zinc oxide nanoparticles on *Aspergillus fumigatus* fungus &*Candida albicans* yeast. *Citeseer*, *5*, 23-28.

56. Ananthalakshmi, R., Rajarathinam, S. R., & Sadiq, A. M. (2019). Antioxidant activity of ZnO Nanoparticles synthesized using *Luffa acutangula* peel extract. *Research Journal of Pharmacy and Technology*, *12*(4), 1569-1572.

57. Suresh, P., Doss, A., Praveen Pole, R. P., & Devika, M. (2024). Green synthesis, characterization, and antioxidant activity of bimetallic (Ag-ZnO) nanoparticles using *Capparis zeylanica* leaf extract. *Biomass Conversion and Biorefinery*, *14*(14), 16451-16459.

58. Gulcin, İ., &Alwasel, S. H. (2023). DPPH radical scavenging assay. *Processes*, *11*(8), 2248.

59. Rehana, D., Mahendiran, D., Kumar, R. S., & Rahiman, A. K. (2017). In vitro antioxidant and antidiabetic activities of zinc oxide nanoparticles synthesized using different plant extracts. *Bioprocess and biosystems engineering*, *40*(6), 943-957.

60. Venkatesan, A., Vinoth Raja Antony Samy, J., Balakrishnan, K., Natesan, V., & Kim, S. J. (2023). In vitro antioxidant, anti-inflammatory, antimicrobial, and antidiabetic activities of synthesized chitosan-loaded p-coumaric acid nanoparticles. *Current Pharmaceutical Biotechnology*, *24*(9), 1178-1194.

61. Karthick, V., Zahir, A. A., Ayyanar, M., Amalraj, S., Anbarasan, K., Rahuman, A. A., ... & Tamizharasan, P. (2024). Optimization and characterization of eco-friendly formulatedZnO NPsin various parameters: assessment of its antidiabetic, antioxidant and antibacterial properties. *Biomass Conversion and Biorefinery*, *14*(19), 24567-24581.

62. Nandhini, R., Rajeswari, E., Harish, S., Sivakumar, V., & Gangai Selvi, R. (2025). Role of chitosan nanoparticles in sustainable plant disease management. *J. Nanopart. Res*, *27*, 13.

63. Mani, V., Gopinath, K. S., Varadharaju, N., Wankhar, D., & Annavi, A. (2024). *Abutilon indicum*-mediated green synthesis of NiO and ZnO nanoparticles: Spectral profiling and anticancer potential against human cervical cancer for public health progression. *Nano TransMed*, *3*, 100049.

64. El Sadieque, A., Shawki, M., Elabd, S., & Moustafa, M. (2022). The Cytotoxicity ofZnO NPson Breast Cancer Cell Lines MCF-7 Depending on the Dispersion Solution. *Physics of Particles and Nuclei Letters*, *19*(3), 282-284.

65. Yassin, M. T., Al-Otibi, F. O., Al-Sahli, S. A., El-Wetidy, M. S., & Mohamed, S. (2024). Metal Oxide Nanoparticles as Efficient Nanocarriers for Targeted Cancer Therapy: Addressing Chemotherapy-Induced Disabilities. *Cancers*, *16*(24), 4234.